Available online at www.sciencedirect.com

ScienceDirect

IFAC PapersOnline CONFERENCE PAPER ARCHIVE

IFAC PapersOnLine 52-21 (2019) 8–13

Combined kinematic and dynamic control of an underwater swimming manipulator ⋆

I.-L. G. Borlaug * **J. Sverdrup-Thygeson** * **K. Y. Pettersen** * **J. T. Gravdahl** *

* *Centre for Autonomous Marine Operations and Systems, Department of Engineering Cybernetics, NTNU, Norwegian University of Science and Technology, Trondheim, Norway (e-mail: {Ida.Louise.Borlaug, Jorgen.Sverdrup-Thygeson, Kristin.Y.Pettersen, Tommy.Gravdahl}@ntnu.no).*

Abstract: An underwater swimming manipulator (USM) is a long and slender underwater vehicle composed of multiple links that are connected by motorized joints and equipped with thrusters. The USM belongs to the class of underwater vehicle-manipulator systems (UVMS), and the main task is to carry out autonomous inspections and light intervention operations on subsea installations. To achieve this, it is important to develop a control system that maintains the stability of the USM, while at the same time utilizes the kinematic redundancy of this highly flexible underwater vehicle. In this paper, we propose a combined kinematic and dynamic control approach for the USM. The approach uses the singularity robust multiple task priority (SRMTP) framework to generate a velocity reference and combines this with a dynamic velocity controller based on sliding mode control (SMC). This novel approach allows us to analyze the stability properties of the kinematic and dynamic subsystems together, in the presence of model uncertainty, while still retaining the possibility to solve multiple tasks simultaneously. We show that the multiple set-point regulation tasks will converge asymptotically to zero without the strict requirement that the velocities are perfectly controlled. This novel approach then avoids the assumption of perfect dynamic control that is common in kinematic stability analyses for robot manipulators. We demonstrate the applicability of the proposed approach through a simulation study of a USM carrying out three simultaneous tasks. The results show that all the regulation tasks converge to their respective set-points. The proposed control approach is applicable to vehicle-manipulator systems in general, and for any combination of regulation tasks.

Keywords: Underwater swimming manipulator, inverse kinematic control, sliding mode control, underwater vehicle-manipulator systems, underwater robotics

1. INTRODUCTION

Inspection and intervention operations on subsea installations are typically carried out by an underwater vehicle-manipulator system (UVMS). Remotely operated vehicles (ROVs) and autonomous underwater vehicles (AUVs) are the most common examples of a UVMS. A recent addition to this family of underwater vehicles is the underwater swimming manipulator (USM) presented in Sverdrup-Thygeson et al. (2018). The USM is a long and slender underwater vehicle composed of multiple links that are connected by motorized joints (see Figure 1). In addition to the actuated joints, the USM is also equipped with thrusters, which give hovering capabilities. With its slender, lightweight, and flexible design, the USM addresses some of the limitations of conventional underwater vehicles. The USM is a specialized type of underwater vehicle, whose main task is to carry out autonomous inspections and light intervention operations. To fulfill this task, it is important to develop a control system that maintains the stability of the USM, while at the same time utilizes the kinematic redundancy of this highly flexible underwater vehicle.

A common way of developing a control system for a UVMS is to design standalone control laws for the kinematic part and the dynamic part, and to analyze the stability properties of the two subsystems separately. When analyzing the stability properties of the kinematic subsystem, it is common to neglect the dynamics and assume that the reference output is tracked perfectly by the dynamic controller. In practice, this assumption is often justified by stating that the dynamic control loop is faster than the kinematic one. This makes sense for fixed-base manipulators or when the mass of the vehicle is much larger than the mass of the manipulator arm, so that the joint motion does not have a significant impact on the overall motion of the whole vehicle. For the USM, it is not sufficient to rely on this assumption due to the large coupling effects. Inertia, drag forces, and restoring forces and moments caused by the

⋆ This research was partly funded by the Research Council of Norway through the Centres of Excellence funding scheme, project No. 223254 NTNU AMOS, and partly funded by VISTA, a basic research program in collaboration between The Norwegian Academy of Science and Letters, and Statoil.

10.1016/j.ifacol.2019.12.275

joint motion have a significant effect on the overall motion of the whole mechanism. Indeed, for this type of system, it is necessary to analyze the stability properties of the kinematic and the dynamic subsystems together.

One possible approach is to combine second-order inverse kinematics with feedback linearization (Schjølberg and Egeland, 1996). This method integrates the inverse kinematic control with the dynamic control loop and analyzes the stability properties of the integrated system. However, feedback linearization requires perfect knowledge of the model parameters, as well as perfect measurements of both position, attitude, joint angles, and velocities. Also, the possibility to utilize the kinematic redundancy of the system is somewhat limited with this method, and the method is prone to algorithmic singularities caused by non-compatible tasks.

In this paper, we propose a novel approach for analyzing the stability properties of the kinematic and the dynamic subsystems together, in the presence of model uncertainty, while still retaining the possibility to solve multiple tasks simultaneously. The main idea is to combine the singularity robust multiple task priority (SRMTP) framework (Chiaverini, 1997) with a robust sliding mode controller, and at the same time ensure that the task errors remain bounded. The kinematic stability analysis of the SRMTP method is based on the results in Antonelli (2009). The proposed sliding mode controller is a velocity controller which is able to track a velocity reference vector. This reference vector is here chosen as the output from the SRMTP inverse kinematics controller. Part of the analysis of the sliding mode controller is based on Antonelli and Chiaverini (1998), which considers a set-point regulation problem for a UVMS without taking into account the inverse kinematic problem. In this paper, we modify the analysis in Antonelli and Chiaverini (1998) to show finite time convergence of the velocity controller. This property then allows us to show that the multiple set-point regulation tasks will converge asymptotically to zero without the strict requirement that the velocities are perfectly controlled. This novel approach then avoids the assumption of perfect dynamic control that is common in kinematic stability analyses for robot manipulators. The proposed method is illustrated with a simulation study, where the primary task is the position and orientation of the center link of the USM, and the secondary tasks are the orientation of the front end and the back end of the USM.

The remainder of this paper is structured as follows. The mathematical model of the USM is presented in Section 2, and a quick introduction to inverse kinematic control and the SRMTP method is provided in Section 3. The main stability analysis is described in Section 4 and demonstrated with a simulation study in Section 5. Conclusions are drawn in Section 6.

2. USM MODEL

For control purposes, the USM is considered as a floating base manipulator operating in an underwater environment. The complete dynamic model of the USM, including hydrodynamic forces, hydrostatic forces, and actuator forces, can then be written with the same structure as a typical underwater vehicle-manipulator system (Antonelli, 2014), (Schjølberg and Fossen, 1994)

$$M(q)\dot{\zeta} + C(q,\zeta)\zeta + D(q,\zeta)\zeta + N(R_{Ic},q) = \tau, \quad (1)$$

where $M(q) = M_A(q) + M_{RB}(q)$ and $C(q,\zeta) = C_A(q,\zeta) + C_{RB}(q,\zeta)$, $M_A(q)$ is the added inertia matrix, $M_{RB}(q)$ is the rigid body inertia matrix, $C_A(q,\zeta)$ is the added Coriolis-centripetal matrix, $C_{RB}(q,\zeta)$ is the rigid body Coriolis-centripetal matrix, $D(q,\zeta)$ is the damping matrix, and $N(R_{Ic},q)$ is the vector of gravitational and buoyancy forces. The generalized forces and moments, τ, created by the thrusters and the joint motors are given by

$$\tau = \tau_{thr}(q) + \tau_q = \begin{bmatrix} T(q) & 0 \\ T_q(q) & I_{n\times n} \end{bmatrix} \begin{bmatrix} f_{thr} \\ u_q \end{bmatrix} = Bu. \quad (2)$$

The dynamic model in (1) can be formulated with respect to a coordinate frame having its origin at an arbitrary position on the USM. In this paper, we assume that the model is formulated with respect to the center link of the USM, such that the velocity state vector, ζ, is defined by

$$\zeta = \begin{bmatrix} v_{Ic}^c \\ \omega_{Ic}^c \\ \dot{q} \end{bmatrix} \in \mathbb{R}^{6+n} \quad (3)$$

where v_{Ic}^c and ω_{Ic}^c are the body-fixed linear and angular velocities of the center link of the USM, respectively, and $\dot{q}$ is the vector of joint velocities. A detailed derivation of the USM model can be found in Sverdrup-Thygeson et al. (2018).

Remark 1. The formulation in (1) preserves the following important properties (From et al., 2014):

(1) $M = M^T > 0$
(2) $x^T(\dot{M} - 2C)x = 0$
(3) $x^T D x > 0$

3. INVERSE KINEMATIC CONTROL

Robot manipulators are designed to perform specific tasks associated with either the internal configuration of the robot (joint/configuration space) or the external configuration with respect to the environment (operational/task space). A task that specifies a desired position and/or orientation for the end-effector of the robot is an example of a common operational space task. A comprehensive collection of possible tasks for underwater robotic vehicles is presented in Antonelli (2014). An m-dimensional task can be described by the task variable, $\sigma(t) \in \mathbb{R}^m$, and defined by

$$\sigma(t) = f(\xi(t)), \quad (4)$$

where $\xi(t) \in \mathbb{R}^n$ is the n-dimensional vector of generalized coordinates describing the configuration of the robot manipulator, and $f(\cdot)$ is a function that maps the configuration into the task space coordinates. The generalized coordinates $\xi(t)$ can be the joint angles of a fixed-base robot, the position and orientation of a single body vehicle, or both for a floating base manipulator such as the USM.

Let $\sigma_{i,d}(t) \in \mathbb{R}^m$ be the desired trajectory for the task variable $\sigma_i(t)$ and define the task error $\tilde{\sigma}_i \in \mathbb{R}^m$ as

$$\tilde{\sigma}_i = \sigma_{i,d} - \sigma_i. \quad (5)$$

To determine the motion required to achieve convergence of the task error $\tilde{\sigma}$ to zero it is common to use the closed-loop inverse kinematic (CLIK) routine expressed by

$$\zeta_r = J^+(\dot{\sigma}_{i,d} + \Lambda_i \tilde{\sigma}_i), \quad (6)$$

where $J^+ = J^T(JJ^T)^{-1}$ is the right Moore-Penrose pseudo-inverse of the task Jacobian, ζ_r is the reference velocity vector and $\Lambda_i > 0$ is a positive-definite gain matrix. The single task approach can be extended to multiple simultaneous tasks using the SRMTP method (Chiaverini, 1997)

$$\begin{aligned}\zeta_r =& J_1^+ \left(\dot{\sigma}_{1,d} + \Lambda_1 \tilde{\sigma}_1\right) + N_1 J_2^+ \left(\dot{\sigma}_{2,d} + \Lambda_2 \tilde{\sigma}_2\right) \\ &+ \ldots + N_{12..(k-1)} J_k^+ \left(\dot{\sigma}_{k,d} + \Lambda_k \tilde{\sigma}_k\right),\end{aligned} \tag{7}$$

where the null spaces of the task Jacobians are given by $N_i{=}(I - J_i^+ J_i)$, and $N_{12..(k-1)}{=}\text{Null}(\left[J_1^T, J_2^T, \ldots, J_{k-1}^T\right]^T)$ represents the combined null space of tasks 1 through $k-1$. The null space matrices ensure that conflicting velocity components generated by the lower priority tasks are filtered out. In Antonelli (2009), it is shown that all the task errors will converge to zero, provided that $\zeta = \zeta_r$ (neglecting the dynamics), that the tasks are compatible and specified as time-independent regulation tasks ($\dot{\sigma}_{i,d} = 0$), and that the task gains Λ_i are chosen appropriately.

In the next section, we extend the kinematic stability analysis in Antonelli (2009) by combining it with a dynamic control law for the USM model described in Section 2.

4. COMBINED KINEMATIC AND DYNAMIC STABILITY ANALYSIS

In this section, we propose a combined kinematic and dynamic control law for a USM carrying out an arbitrary number of regulation tasks. By combining the Lyapunov analysis for time-independent regulation tasks presented in Antonelli (2009) with a sliding mode controller, we show that all the regulation task errors will converge asymptotically to zero without the strict requirement that $\zeta(t) = \zeta_r(t)\ \forall\, t \geq 0$. This novel approach then avoids the assumption of perfect dynamic control that is common in kinematic stability analyses for robot manipulators. The following theorem establishes the convergence properties of the proposed control law.

Theorem 1. Let $\zeta_r = \left[(v_{Ic,r}^c)^T\ (\omega_{Ic,r}^c)^T\ \dot{q}_r^T\right]^T \in \mathbb{R}^{6+n}$ be a reference velocity vector given as the output of the SRMTP inverse kinematics routine in (7) for time-independent regulation tasks:

$$\zeta_r = J_1^+ \Lambda_1 \tilde{\sigma}_1 + N_1 J_2^+ \Lambda_2 \tilde{\sigma}_2 + \ldots + N_{12..(k-1)} J_k^+ \Lambda_k \tilde{\sigma}_k, \tag{8}$$

with $\tilde{\sigma} = \left[\tilde{\sigma}_1^T, \ldots, \tilde{\sigma}_k^T\right]^T$ defined as a vector of all the regulation task errors. Define the sliding variable

$$s \triangleq \zeta - \zeta_r \tag{9}$$

and assume that the thruster configuration matrix $T(q)$ is full rank for all attainable joint configurations. Let the control input of (1-2) be given by the sliding mode control law

$$u = B^\dagger \left[\hat{N}(R_{Ic}, q) - K_d s - K\,\text{sgn}(s)\right], \tag{10}$$

where $K_d > 0$, $\hat{N}(R_{Ic}, q)$ represents the estimate of the gravity/buoyancy forces and moments, and

$$\text{sgn}(s_i) = \begin{cases} 1, \text{ for } s_i \geq 0 \\ -1, \text{ for } s_i < 0 \end{cases}$$

The gain K is taken as

$$K \geq \kappa + K_0, \tag{11}$$

where $K_0 > 0$ and κ is an upper bound chosen to satisfy

$$\kappa \geq ||C(q,\zeta)\zeta_r + D(q,\zeta)\zeta_r + \tilde{N}(R_{Ic}, q) + M(q)\dot{\zeta}_r||. \tag{12}$$

The sliding variable s will converge exponentially and in finite time to the sliding surface, $s = 0$, which then ensures asymptotic convergence of the regulation task errors, that is

$$\lim_{t\to\infty} \tilde{\sigma}(t) = 0.$$

Proof. Consider the Lyapunov function candidate (LFC)

$$V_s = \frac{1}{2} s^T M s > 0, \quad \forall s \neq 0, \tag{13}$$

which is positive definite as $M(q) > 0$. Differentiating (13) and inserting $s = \zeta - \zeta_r$, $\dot{s} = \dot{\zeta} - \dot{\zeta}_r$, and (1) yields

$$\begin{aligned}\dot{V}_s &= s^T M \dot{s} + \frac{1}{2} s^T \dot{M} s \\ &= s^T \left[Bu - C\zeta - D\zeta - N - M\dot{\zeta}_r\right] + \frac{1}{2} s^T \dot{M} s \\ &= -s^T D s + s^T \left[Bu - C\zeta_r - D\zeta_r - N - M\dot{\zeta}_r\right] \\ &\quad + \frac{1}{2} s^T \left[\dot{M} - 2C\right] s.\end{aligned} \tag{14}$$

The last term in (14) is equal to zero because $\dot{M} - 2C$ is skew-symmetric, as shown in From et al. (2014). Inserting (10) yields

$$\begin{aligned}\dot{V}_s =& -s^T(K_d + D)s - s^T\left[K\,\text{sgn}(s)\right] \\ &+ s^T\left[-C\zeta_r - D\zeta_r - \tilde{N} - M\dot{\zeta}_r\right] \\ \leq& -s^T(K_d + D)s - K||s|| \\ &+ ||C\zeta_r + D\zeta_r + \tilde{N} + M\dot{\zeta}_r||||s||,\end{aligned} \tag{15}$$

where we have used the Cauchy-Schwarz inequality. Inserting (12), we have that

$$\dot{V}_s \leq -s^T(K_d + D)s - K_0||s|| < 0, \quad \forall s \neq 0. \tag{16}$$

The first term in (16) ensures exponential convergence towards the sliding surface $s = 0$, while the second term ensures, by use of the comparison lemma (Khalil, 2002, Lemma 3.4), that s reaches the sliding surface in finite time. Thus, we have exponential and finite time convergence to the sliding surface.

In Antonelli (2009), it is shown that if the generalized velocities of the robot follow the reference velocities, then the regulation task errors asymptotically converge to zero, i.e. $\lim_{t\to\infty} \tilde{\sigma}(t) = 0$. This corresponds to the assumption that $\zeta = \zeta_r$. The stability proof is carried out using the Lyapunov function $V(\tilde{\sigma}) = \frac{1}{2}\tilde{\sigma}^T\tilde{\sigma}$. In this paper, we also include the dynamic control part of the problem. According to (16), the dynamic control part of the system is finite time stable, which means that $\zeta = \zeta_r$ after a finite time T. This also implies that $||s|| \leq \delta\ \forall\, t \geq 0$, where δ is a positive constant. However, since the drag forces and the restoring forces and moments caused by the joint motion and the thrusters have a significant effect on the overall motion of the USM, we must also check that the task errors do not escape to infinity before $\zeta = \zeta_r$. To prove the boundedness of the task errors we use the same LFC $V(\tilde{\sigma}) = \frac{1}{2}\tilde{\sigma}^T\tilde{\sigma}$. Now, instead of assuming that $\zeta = \zeta_r$ as done in Antonelli (2009), we use $\zeta = \zeta_r + s$. By defining the vector of regulation task errors as $\tilde{\sigma} = \sigma_d - \sigma$ we have that

$$\dot{\tilde{\sigma}} = -\dot{\sigma} = -J(q)\zeta, \tag{17}$$

where $J(q) = \left[J_1^T, J_2^T, \ldots, J_k^T\right]^T$ is a matrix containing the corresponding Jacobian matrices for the tasks. The total error dynamics can then be obtained by combining (1), the derivative of (9) and (17), and using that $\zeta = \zeta_r + s$:

$$\begin{aligned}\dot{\tilde{\sigma}} &= -J(q)\zeta = -J(q)(\zeta_r + s)\\ \dot{s} &= \dot{\zeta} - \dot{\zeta}_r = M(\cdot)^{-1}\big(-C(\cdot)(\zeta_r + s) - \\ &\quad D(\cdot)(\zeta_r + s) - N(\cdot) + \tau\big) - \dot{\zeta}_r.\end{aligned} \tag{18}$$

The derivative of the LFC is then as follows:

$$\dot{V} = \tilde{\sigma}^T\dot{\tilde{\sigma}} = -\tilde{\sigma}^T J(q)(\zeta_r + s) \tag{19}$$

From Antonelli (2009) we have that

$$\tilde{\sigma}^T J(q)\zeta_r = \tilde{\sigma}^T P(q)\tilde{\sigma}, \tag{20}$$

where $P(q)$ is defined as

$$P(q) = \begin{bmatrix} \Lambda_1 & O_{m_1,m_2} & \ldots & O_{m_1,m_k} \\ J_2 J_1^+ \Lambda_1 & J_2 N_1 J_2^+ \Lambda_2 & \ldots & J_2 \bar{N} J_k^+ \Lambda_k \\ \ldots & \ldots & \ldots & \ldots \\ J_{k-1} J_1^+ \Lambda_1 & J_{k-1} N_1 J_2^+ \Lambda_2 \ldots & J_{k-1}\bar{N} J_k^+ \Lambda_k \\ J_k J_1^+ \Lambda_1 & J_k N_1 J_2^+ \Lambda_2 & \ldots & J_k \bar{N} J_k^+ \Lambda_k \end{bmatrix} \tag{21}$$

where $\bar{N} = N_{12..(k-1)}$. By using (20) we can write the LFC derivative as

$$\dot{V} = -\tilde{\sigma}^T P(q)\tilde{\sigma} - \tilde{\sigma}^T J(q)s \tag{22}$$

Since we have proven above that $||s(t)|| \leq \delta \ \forall t \geq 0$, we can rewrite the LFC such that it becomes

$$\begin{aligned}\dot{V} &\leq -\lambda_{\min}(P)||\tilde{\sigma}||^2 + \delta||J(q)||||\tilde{\sigma}|| \\ &= -\lambda_{\min}(P)||\tilde{\sigma}||^2 + \theta||\tilde{\sigma}||^2 - \theta||\tilde{\sigma}||^2 + \delta||J(q)||||\tilde{\sigma}|| \\ &\leq -(\lambda_{\min}(P) - \theta)||\tilde{\sigma}||^2 \quad \forall \quad ||\tilde{\sigma}|| \geq \frac{\delta||J(q)||}{\theta}\end{aligned} \tag{23}$$

where $0 < \theta < \lambda_{\min}(P)$, since P is positive definite (Antonelli, 2009). The regulation task errors are then bounded as long as $J(q(t))$ is bounded, because then the conditions of (Khalil, 2002, Theorem 4.18) are satisfied. Consequently, the regulation task errors will asymptotically converge to zero, i.e. $\lim_{t\to\infty}\tilde{\sigma}(t) = 0$, since they do not escape to infinity while $s \neq 0$. Note that the matrix $J(q(t))$ will be bounded as long as singularities in the task representations are avoided.

Remark 2. To determine κ we need to find an upper bound on the expression in (12). This upper bound depends on the size of the task errors. A reference model (Fossen, 2002) can be used to obtain sufficiently smooth desired trajectories and avoid large jumps in the task errors when changing set-points. Such a reference model can also include saturating elements to limit the desired velocities.

Remark 3. The analysis presented above assumes ideal actuators. In practice, time delays and imperfections in the actuators will cause high-frequency chattering when sliding mode control is applied. To eliminate the chattering problem, the discontinuous signum function in (10) is typically replaced by a high-slope saturation function. In that case, we achieve ultimate boundedness of the task errors. For set-point regulation problems, integral action can be introduced in the control law to achieve zero steady-state error (Khalil, 2002).

Remark 4. This proof can be extended to include trajectory tracking tasks as long as the tasks are orthogonal and the tracking error dynamics is asymptotically stable. Orthogonal tasks is a strict requirement which in practice means that the tasks utilize separate degrees of freedom of the robot.

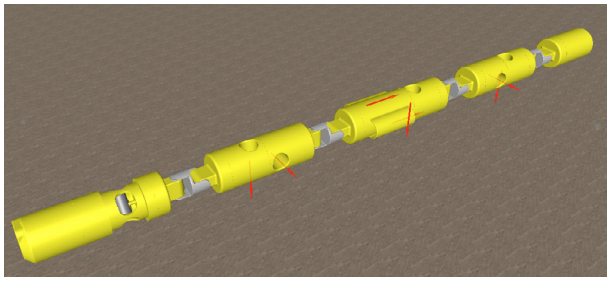

Fig. 1. Vortex simulation model

5. SIMULATION STUDY

In this section, the combined kinematic and dynamic control of the USM is demonstrated using the following three set-point regulation tasks:

(1) Control the position and orientation of the center link (main task)
(2) Control the pitch and the yaw angle of the front end of the USM
(3) Control the pitch and the yaw angle of the back end of the USM

This combination of tasks illustrate the ability of the USM to move to a position of interest and then perform a double observation task by adjusting the pitch and the yaw angles of the back end and the front end of the USM simultaneously.

The simulation of the motion of the USM is performed using the dynamic simulation tool Vortex by CM Labs (CM Labs Simulations Inc., 2019). As visualized in Figure 1, the USM model consists of five links, where each link is connected to its neighboring link by a double joint module consisting of two 1-DOF joints. In addition, the model is equipped with a total of seven thrusters. Passive stability in roll and pitch is introduced by setting the center of gravity of each link 6 cm below the volumetric center. This passive stability is required because the thruster configuration of the simulation model is singular in roll when the USM is straight. A more detailed description of the simulation model is given in Sverdrup-Thygeson et al. (2018).

The task Jacobian for Task 1 is trivial, since it is completely described by the position and orientation of the center link. The second task is fulfilled using the two double joint modules in front of the center link, while the third task utilizes the two double joint modules behind the center link. The available degrees of freedom are split between the tasks. Although this is not necessary, it is a way to ensure that the tasks are compatible, so that all tasks can be fulfilled simultaneously.

The expressions for the task errors and the task Jacobians are:

Task 1 - Position and orientation of the center link

$$\begin{aligned}\tilde{\sigma}_1 &= \left[(\tilde{p}_{Ic}^c)^T, \mathrm{sgn}(\tilde{\eta}_c)\tilde{\epsilon}_c^T\right] \\ J_1 &= \left[I_{6\times 6}\ 0_{6\times 8}\right],\end{aligned}$$

Task 2 - Orientation of the front end

$$\tilde{\sigma}_2 = \begin{bmatrix} 0 & 1 & 0 \\ 0 & 0 & 1 \end{bmatrix} \text{sgn}(\tilde{\eta}_f)\tilde{\epsilon}_f^T$$
$$J_2 = J_{cf}(\text{row 5-6})$$

Task 3 - Orientation of the back end

$$\tilde{\sigma}_3 = \begin{bmatrix} 0 & 1 & 0 \\ 0 & 0 & 1 \end{bmatrix} \text{sgn}(\tilde{\eta}_b)\tilde{\epsilon}_b^T$$
$$J_3 = J_{cb}(\text{row 5-6})$$

where $\tilde{p}_{Ic}^c$ is the position deviation of the center link, $\tilde{\eta}$ and $\tilde{\epsilon}$ represent the components of the unit quaternion deviations for the front end, the back end, and the center link orientations, and J_{cf} and J_{cb} are the front end and back end Jacobians, respectively. These Jacobians relate the body-fixed velocities of the front end and the back end to the body-fixed velocity of the center link and the joint velocities.

The reference velocities, ζ_r, are calculated according to

$$\zeta_r = J_1^+ \Lambda_1 \tilde{\sigma}_1 + N_1 J_{23}^+ \begin{bmatrix} \Lambda_2 & 0 \\ 0 & \Lambda_3 \end{bmatrix} \begin{bmatrix} \tilde{\sigma}_2 \\ \tilde{\sigma}_3 \end{bmatrix}. \quad (24)$$

Task 2 and task 3 are always compatible, which allows us to augment the two task Jacobians into J_{23}. The set-points $\sigma_{i,d}$ are manually controlled and filtered through a third order reference filter to avoid discontinuities and large jumps in the calculated reference velocities. The control law gains for the roll axis is set to zero to avoid excessive control efforts caused by the thruster roll axis singularity. Also, to avoid chattering, the sgn function in (10) is replaced by a high-slope saturation function with a boundary layer.

Figures 2 and 3 show the commanded and the actual position and orientation of the center link, corresponding to task 1. There is a small deviation from the set-point for the center link pitch angle, due to the boundary layer of the saturation function, in agreement with ultimate boundedness as described in Remark 3. The results for tasks 2 and 3 are shown in Figure 4 and Figure 5. We see that the combined kinematic and dynamic control law is able to fulfill all the tasks simultaneously, as stated in Theorem 1, but some transient deviations can be observed for the front and the back orientation when changing the pitch and yaw set-points for the center link. These deviations occur because task 1 is the primary task and tasks 2 and 3 are secondary tasks. The first term in (24) does not consider the task errors for tasks 2 and 3. Satisfying the desired center link orientation will therefore introduce errors in the orientation of the front end and the back end. The deviations disappear as soon as the second term in (24) compensates for these task errors. We can also see transient deviations in the front end orientation when the back end orientation is changed, and vice versa. These deviations appear because of coupling forces caused by the joint motion, and not because the tasks are not compatible, since when the front end and back end reach their set-points the opposite end converge to its respective set-point. At around 650s the front and back pitch errors are especially large, this is probably because the center link, front end and back end orientations are changed simultaneously, which causes multiple joints to move at the same time, and therefore results in large coupling forces. The simulation results support the theoretical results, and we see that all the set-point tasks are fulfilled.

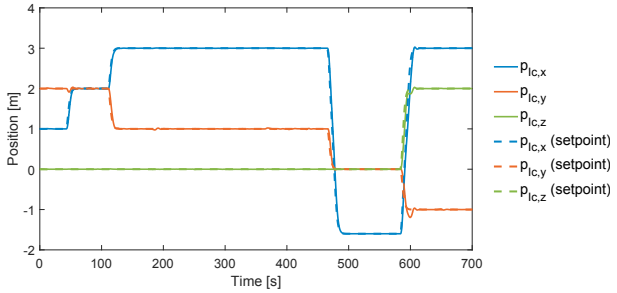

Fig. 2. Center link position

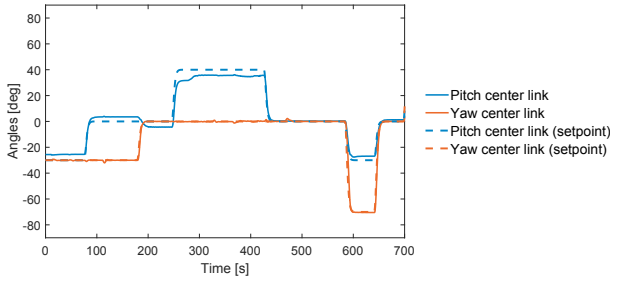

Fig. 3. Center link orientation

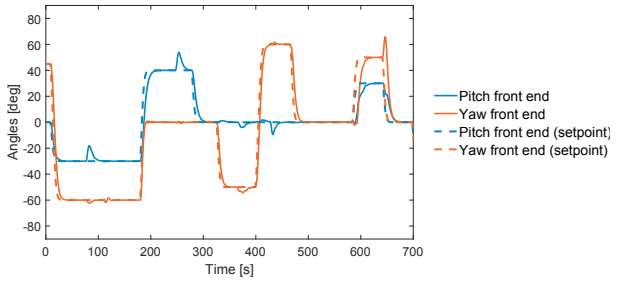

Fig. 4. Front end orientation

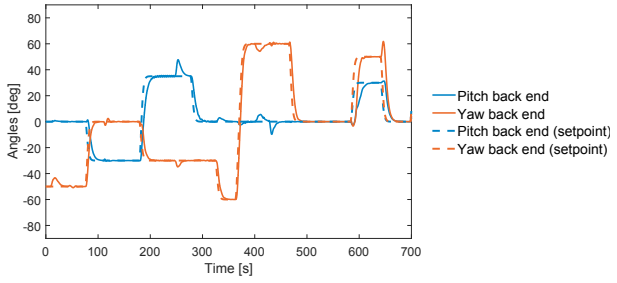

Fig. 5. Back end orientation

6. CONCLUSIONS

In this paper, we have proposed a combined kinematic and dynamic control approach for floating base manipulators, such as the USM, and presented an extended stability analysis for multiple set-point regulation tasks. The method extends previous stability analyses, and shows that the multiple set-point regulation tasks will converge asymptotically to zero without the strict requirement that the velocities are perfectly controlled. This novel approach then avoids the assumption of perfect dynamic control that is common in kinematic stability analyses for robot manipulators. The applicability of the method is demonstrated through a simulation study of a USM carrying out three simultaneous tasks, and the results show that all the

regulation tasks converge to their respective set-points. The proposed control approach is applicable to vehicle-manipulator systems in general, and for any combination of regulation tasks.

REFERENCES

Antonelli, G. (2009). Stability analysis for prioritized closed-loop inverse kinematic algorithms for redundant robotic systems. *IEEE Transactions on Robotics*, 25(5), 985–994.

Antonelli, G. (2014). *Underwater Robots*. Springer International Publishing, 3rd edition.

Antonelli, G. and Chiaverini, S. (1998). Singularity-free regulation of underwater vehicle-manipulator systems. In *Proc. American Control Conference*, 399–403. Philadelphia, PA, USA.

Chiaverini, S. (1997). Singularity-robust task-priority redundancy resolution for real-time kinematic control of robot manipulators. *IEEE Transactions on Robotics and Automation*, 13(3), 398–410.

CM Labs Simulations Inc. (2019). Vortex simulation software.

Fossen, T.I. (2002). *Marine Control Systems - Guidance, Navigation, and Control of Ships, Rigs, and Underwater Vehicles*. Marine Cybernetics, Trondheim.

From, P.J., Gravdahl, J.T., and Pettersen, K.Y. (2014). *Vehicle-Manipulator Systems: Modeling for Simulation, Analysis, and Control*. Advances in Industrial Control. Springer.

Khalil, H.K. (2002). *Nonlinear Systems*. 3rd ed. Prentice Hall.

Schjølberg, I. and Egeland, O. (1996). Motion control of underwater vehicle-manipulator systems using feedback linearization. *Modeling, Identification, and Control*, 17(1), 17–26.

Schjølberg, I. and Fossen, T.I. (1994). Modelling and control of underwater vehicle-manipulator systems. In *Proc. 3rd Conf. on Marine Craft Maneuvering and Control*, 45–57. Southampton, UK.

Sverdrup-Thygeson, J., Kelasidi, E., Pettersen, K.Y., and Gravdahl, J.T. (2018). The underwater swimming manipulator - a bioinspired solution for subsea operations. *IEEE Journal of Oceanic Engineering*, 43(2), 402–417.